Vol. 10(2), pp. 19-37, July-December, 2024
DOI: 10.5897/IJCER2023.0309
Article Number: CD1B00272341
ISSN: 2141-6494

http://www.academicjournals.org/IJCER

ACADEMIC JOURNALS
expand your knowledge

International Journal of Computer Engineering Research

Review

Modelling, simulation and optimisation of a pressure retarded osmosis power station: The co- vs. counter-current setting

O. O. Bolorunduro and I. Gasser*

Department of Mathematics, Universitat of Hamburg, Bundesstrasse 55, 20146 Hamburg, Germany.

Received 18 September, 2023; Accepted 8 March, 2024

In a pressure retarded osmosis (PRO) power plant, osmosis is used to generate electric power in a 2-channel system through a semipermeable membrane. Such system can be operated in the co- or in the counter-current mode, depending on relative flow direction of the fresh and the salt (draw) water along the membrane. In order to study and compare these two cases, models which describe the variations of the various quantities across the membrane are needed. The variations across the membrane have become relevant, particularly in transition from lab-scale PRO systems to real scale PRO systems. Based on a recently developed model, we simulate and optimize the co- and the counter-current case, compare the two cases and compare the results to other available examples from the literature. We optimize the power and the power per volume ratio with respect to both operational parameters such as applied pressures and with respect to geometric and membrane parameters. The results predict an advantage.

Key words: Pressure retarded osmosis (PRO), co and counter-current mode, semi-permeable membrane, mass flow rate, power density, specific energy.

INTRODUCTION

As a reaction to climate change, many alternatives and renewable energy sources are considered. It is well known that pressure retarded osmosis (PRO) can be such a possible alternative. PRO is well understood on a theoretical level (Achilli and Childress, 2010, Logan and Elimelech, 2012, Kim et al., 2015). In addition, a working prototype power plant operated by the Norwegian company-Statkraft has shown the practical realization (Achilli and Childress, 2010; Gerstandt et al., 2008, Torleif and Thorsent, 2009).

The idea of PRO is to bring in contact, fresh (sweet) and salt water in the “core” membrane unit along a semipermeable membrane (Figure 1). Then, osmosis under appropriate pressure conditions “pumps” fresh water through the membrane to the salt water part, dilutes and increases the flow in the salt water part. This additional flow is used to power a turbine and to produce electricity. To run such a system, the water in the fresh and the salt water part have to be pumped in, to guarantee the appropriate pressure conditions.

*Corresponding author. E-mail: ingenuin.gasser@uni-hamburg.de.

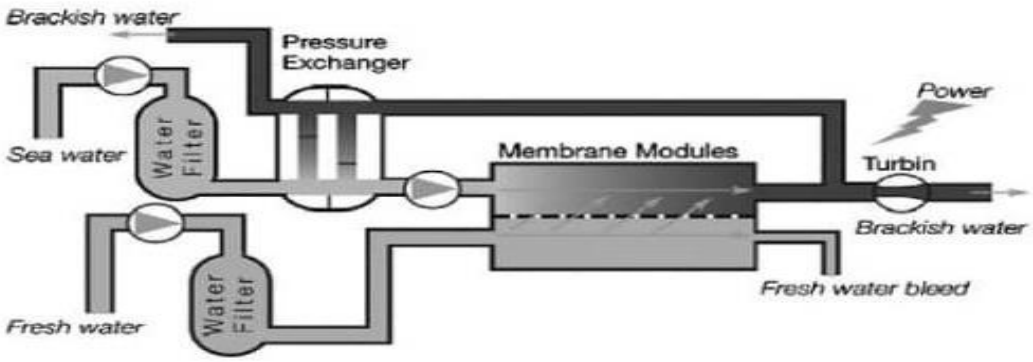

Figure 1. Schematic representation of the PRO power plant by Statkraft (Ahmed and Rohini, 2012).

Nevertheless, the generated energy in the turbine is more than the consumed energy in the pumps and thus a positive net power output is generated.

The first paper with the idea to produce energy via osmosis is due to Pattle, 1954. Starting from the 1970s, models for PRO have been developed (Norman, 1974; Lee et al., 1981; Loeb, 1976, Loeb and Norman, 1975; Pattle, 1974). In (Lee et al., 1981) a schematic view close to the modern realisations has been shown. Also, the first model approaches for flow through the membrane, the permeate flow, can be found in that paper. A review on the history of PRO is given by Achilli and Childress (Achilli and Childress, 2010) and Logan and Elimelech (Logan and Elimelech, 2012).

Recently, in the last two decades, more detailed models have been developed. One important step was to describe the variation of the quantities (densities, flows, pressures) along the membrane (in this paper denoted as the x-coordinate) (Lin et al., 2014; Straub et al., 2014); Maisonneuve et al., 2015; Struchtrup (2014), Yang et al., 2018; Di Michele et al., (2019). Besides the classical co-current setting in some papers, also the counter-current setting is considered (Lin et al., 2014; Straub et al., 2014: Straub et al., 2014). Another fundamental step was to become more realistic in the description and to include non ideal effects such as reverse salt flow (RSF) and internal concentration polarisation (ICP). Most of the models still use the pressure not as an independent (unknown) but as a given input variable. Maison et al. (2015) introduce the pressure as a new independent and coupled variable. However, the model in flow direction is a discrete model (Maisonneuve et al., 2015). A 2-dimensional model with pressure as independent variable is presented in Sung-Soo et al. ((2014) and Sundaramoorthy et al. (2011). Wang et al., (2016) use a continuous model along the membrane in flow direction and for the pressure an averaged value is used.

Recently, more and more non-ideal effects such as friction are introduced in the models (Maisonneuve et al., 2015; Wang et al., 2016; Di Michele et al., 2019). Very early in theoretical considerations, the power output for PRO has been considered (Norman, 1974; Di Michele et al., 2019). Later, in (Achilli et al., 2009; Achilli et al., 2009), more detailed studies were performed. In the last decade also, the specific energy became a quantity of interest (Straub et al., 2014; Lin et al., 2014). In O'Toole et al. (2016), an energy efficiency analysis is presented. Recently, the distinction between net and gross power has become an issue (Maisonneuve et al., 2015; Wang et al 2016; Di Michele et al., 2019). And, more and more optimisation tasks can be found in the literature (Ruiz-Garcia et al., 2022; Chen et al., 2019).

An interesting application is to use a PRO system to increase the efficiency in a sweet water reverse osmosis SWRO system designed for the sweet water production (Senthil and Senthilmurugan, 2016). Applications where various modules are combined can be found in (Ruiz-Garcia et al., 2022). Results on multi-stage PRO are given in (Bharadwaj et al., 2016). PRO as a energy storage system was considered in (Bharadwaj and Struchtrup, 2017).

There is also various recent articles studying the potential and the challenges of PRO (Abdelkader and Sharqawy, 2022; Alzainati et al., 2021).

In Di Michele et al. (2019), one of the most complete continuous models with many of the mentioned features was presented for the co-current setting. The model from (Di Michele et al., 2019) serves as a basis for the studies in this paper. To summarize the features of our model:

(1) resolves the x-dependencies of all variables (along the membrane), relevant for real-scale systems,
(2) couples the flow equations to the pressure equations for the unknown pressures along x,
(3) includes friction losses along the membrane,
(4) considers physically reasonable boundary conditions,
(5) includes the losses of the pumps,
(6) can be adapted easily to the counter-current case,
(7) describes the net power output,
(8) describes the net specific energy,

Table 1. Membrane parameters.

Quantity	Symbol	Value	Unit
Water permeability	A	2.5×10^{-9}	s/m
ICP mass transfer coefficient	K	1×10^{2}	m^2s/kg
Salt Rejection coefficient	R	0.94	1
Temperature	T	297	K
Height	H	1×10^{-3}	m
Length	L	2	m
Width	Y	1	m

Table 2. Physical constants and used fixed parameters.

Quantity	Symbol	Value	Unit
molecular mass of water	M_w	18	kg/kmol
molecular mass of salt	M_s	58.44	kg/kmol
mass density of water	ρ_w	1000	kg/m^3
mass density of salt	ρ_s	2165	kg/m^3
Water gas constant	R_w	462	J/kgK
Temperature	T	297	K
Saltwater viscosity	σ	1.3×10^{-3}	kg/(ms)
Incoming Salinity	$CLd = QLsd/QLwd$	35/983	
Incoming saltwater salt mass fraction	$QLsd/QLd$	35/1018	
Incoming saltwater water mass fraction	$QLwd/QLd$	983/1018	
Pump and turbine efficiency	$\eta T = \eta p$	95%	

(9) allows for fast and robust simulations using state-of-the-art numerical tools, allows to optimize quantities, that is, the net power output or net specific energy.

The presented model has mainly two application areas, the phase where such a power plant is planned and the phase when a given power plant has to be operated in optimal conditions. In this paper, we adapt this model also to the counter-current setting. Our main focus lies in comparing the co- and the counter-current flow setting. In addition, we use various membrane data sets from the literature and compare them.

Mathematically, the optimisation task leads to a constraint optimisation problem. E.g. the net power output or the speciifc energy is optimized and the parameter dependent system of nonlinear ordinary differential equations (ODE) describing the membrane unit, completed with boundary conditions acts as constraints. A list of symbols is given in Appendix 1.

MATHEMATICAL MODEL

The co-current case

Here, we present the mathematical model we want to use to model, simulate and optimize a PRO power station. The model was derived and presented in (Di Michele et al., 2019). The model studies a complete power station with membrane unit, the two pumps and the turbine (Figure 1). The model describes various flow quantities along the flow direction in both the freshwater (feed) and the saltwater (draw) side. The width of the membrane is considered in the sense that all flow quantities are assumed to be homogeneous orthogonal to the flow direction. In this paper, we use membrane parameters from (Lee et al., 1981) collected in Table 1. These parameters were also used in (Di Michele et al. (2019) and (Bolorunduro, 2021). Subsequently, we will consider alternative sets of parameters from (Straub et al., 2014) and (Maisonneuve et al., 2015). The related physical constants and used quantities are given in Table 2.

In the following, we use mass flow rates and mass fluxes (and not volume rates and fluxes). The water permeability A here is given in $kgs^{-1}m^{-2}Pa^{-1} = sm^{-1}$, similar for the ICP mass transfer coefficient, given in m^2skg^{-1}.

We start with the various mass flow rates, water and salt (first index), feed and draw mass (second index) denoted by $I_{wf}(x)$, $I_{wd}(x)$, $I_{sf}(x)$, $I_{sd}(x)$ as functions of x, along the membrane from $x = 0$ to $x = L$, respectively.

These are given in kgs^{-1} and are intended as mass flow rates through a rectangle of channel height H and channel width Y. Due to the assumed homogeneity orthogonal to the flow direction, we consider the related mass flow rates per width, denoted by $Q = \frac{I}{Y}$ width unit $kgs^{-1}m^{-1}$.

The unknown quantities of the model are the feed and draw water (mass) flow rates per width $Q_{wf} = Q_{wf}(x)$, $Q_{wd} = Q_{wd}(x)$, as functions of x, the feed and draw salt mass flow rates per width $Q_{sf} = Q_{sf}(x)$, $Q_{sd} = Q_{sd}(x)$, and the total feed and draw mass flow rates per width is:

$$Q_f(x) = Q_{sf}(x) + Q_{wf}(x),\ Q_d(x) = Q_{sd}(x) + Q_{wd}(x) \quad (1)$$

The (total) feed and draw densities $\rho_f(x)$, $\rho_d(x)$ (in kgm^{-3}) are defined as:

$$\rho_d(x) = \frac{Q_{sd}(x) + Q_{wd}(x)}{\frac{Q_{sd}(x)}{\rho_s} + \frac{Q_{wd}(x)}{\rho_w}}, \quad \rho_f(x) = \frac{Q_{sf}(x) + Q_{wf}(x)}{\frac{Q_{sf}(x)}{\rho_s} + \frac{Q_{wf}(x)}{\rho_w}}.$$

The quantities ρ_w and ρ_s are the mass densities of water and salt, respectively (Table 2). The feed and draw pressures are denoted by $P_f(x)$, $P_d(x)$ (in Pa), respectively. Finally, we have the permeate salt and water mass fluxes (through the membrane) $J_{s,in}(x)$, $J_{w,in}(x)$ (in $kgs^{-1}m^{-2}$), respectively .

The model describes a stationary situation on the interval x ∈ (0, L) and reads as follows (Di Michele et al., 2019):

$$\begin{aligned}
\frac{dQ_{sd}(x)}{dx} &= -J_{s,in}(x),\\
\frac{dQ_{wd}(x)}{dx} &= J_{w,in}(x),\\
\frac{dQ_{sf}(x)}{dx} &= J_{s,in}(x),\\
\frac{dQ_{wf}(x)}{dx} &= -J_{w,in}(x),\\
\frac{dP_d(x)}{dx} &= -\frac{f_{mix,d}(x)}{2H^2}\frac{1}{D_{HY,rect}}\frac{Q_d(x)|Q_d(x)|}{\rho_d(x)} - \frac{1}{H^2}\frac{d}{dx}\left[\frac{Q_d(x)^2}{\rho_d(x)}\right],\\
\frac{dP_f(x)}{dx} &= -\frac{f_{mix,f}(x)}{2H^2}\frac{1}{D_{HY,rect}}\frac{Q_f(x)|Q_f(x)|}{\rho_f(x)} - \frac{1}{H^2}\frac{d}{dx}\left[\frac{Q_f(x)^2}{\rho_f(x)}\right]
\end{aligned} \quad (3)$$

where $D_{HY,rect} = 2\frac{HY}{Y+H}$, the hydraulic diameter of the rectangular flow channel. The first 4 equations are (stationary) mass balance equations. The remaining 2 equations are (time independent) momentum balance equations in the draw and the feed channel, respectively. The first term on the right hand side of the momentum balance describes the friction of the surface, the second term is the convective term.

The function f_{mix} is defined implicitly by the Reynolds number Re_H of the related flow rates per width $Q_d(x)$ or $Q_f(x)$:

$$Re_{H,d/f}(x) = \frac{I_{d/f}(x)}{\sigma HY} D_{HY,rect} = 2\frac{Q_{d/f}(x)}{\sigma Y}\frac{1}{Y+H}, \quad (4)$$

$$f_{mix,d/f}(x) = \frac{96}{Re_{H,d/f}(x)}\left(4.86 + 0.65\sqrt{Re_{H,d/f}(x)}\right) \quad (5)$$

where σ is the salt water viscosity (Table 2).

The system (Equation 3) consists of six coupled ordinary differential equations (ODEs) for the six unknowns Q_{sd}, Q_{wd}, Q_{sf}, Q_{wf}, P_d, P_f. It remains to define the permeate fluxes $J_{s,in}(x)$,$J_{w,in}(x)$.

In the simplest case without any non-ideal effects the permeate salt flux $J_{s,in}(x)$ and the water flux $J_{w,in}(x)$ are defined as:

$$J_{w,in}(x) = A(\Delta\pi(x) - \Delta P(x)), \quad (6)$$
$$J_{s,in}(x) = 0.$$

$\pi_f(x)$ and $\pi_d(x)$ denote the osmotic pressures at feed and draw sides of the membrane, respectively. $\Delta\pi(x) = \pi_d(x) - \pi_f(x)$ and $\Delta P(x) = P_d(x) - P_f(x)$ denote the osmotic and the hydraulic pressure differences between the draw and feed side along the membrane. The osmotic pressurs are defined as (O'Toole et al., 2016):

$$\pi_d = \rho_w R_w T_0 \ln\left(1 - \frac{2M_w}{M_s}\frac{Q_{sd}}{Q_{wd}}\right)^{-1}, \quad \pi_f = \rho_w R_w T_0 \ln\left(1 - \frac{2M_w}{M_s}\frac{Q_{sf}}{Q_{wf}}\right)^{-1}, \quad (7)$$

where M_s, M_w denote the molecular weights of salt and water, respectively. T_0 is the temperature assumed to be constant. R_w gives the water gas constant.

However, to be more realistic, it is necessary to model RSF, ICP and/or ECP effects. Using standard modeling approaches for these effects, we have to modify Equation 6 to

$$\begin{aligned}
J_{w,in}(x) &= A\frac{\Delta\pi(x) - \Delta P(x)\,(1 + KB(x))}{1 + K\,(B(x) + A\pi_f(x))}\\
J_{s,in}(x) &= B(x)\Delta c_{salt}(x),
\end{aligned} \quad (8)$$

where the permeate salt flux does not vanish. The permeate salt flux depends on B given by:

$$B(x) = A\frac{(1-R)(\Delta\pi(x) - \Delta P(x))}{R} \quad (9)$$

with R as salt rejection rate and the difference in the salt concentrations Δc_{salt}

$$\Delta c_{salt}(x) = \frac{Q_{sd}(x)}{Q_d(x)} - \frac{Q_{sf}(x)}{Q_f(x)} \quad (10)$$

The permeate water flux in Equation 8 is also modified. The constant $K = S/D_{salt}$ is the ICP mass transfer coefficient, where S and D_{salt} are the structure parameter and the salt diffusion coefficient of the membrane,

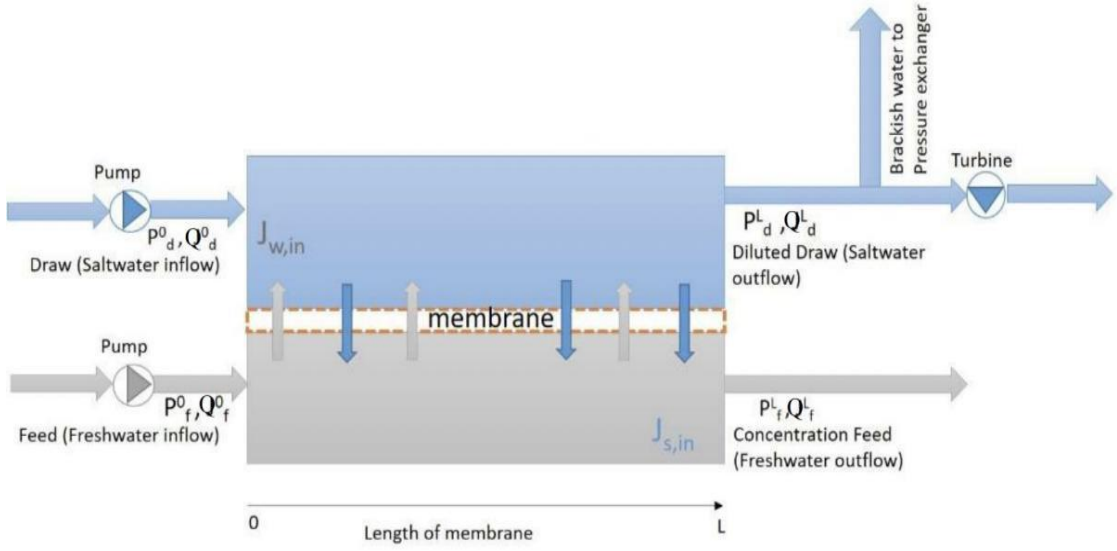

Figure 2. Co-current flow configuration.

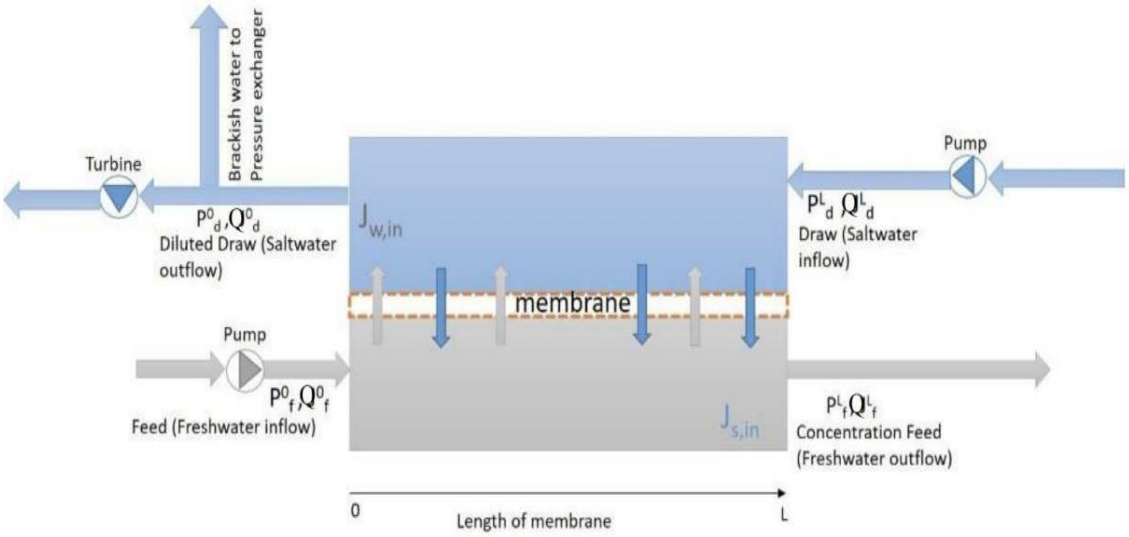

Figure 3. Counter-current flow configuration.

respectively (Lee et al., 1981). This modified form of the permeate water flux in Equation 8 is the result of the solution of a nonlinear relation known from (Lee et al., 1981):

$$J_{w,in} = A\left[\frac{\pi_d - \pi_f e^{KJ_{w,in}}}{1 + \frac{B}{J_{w,in}}(e^{KJ_{w,in}} - 1)} - \Delta P\right]$$

via linearization (Di Michele et al., 2019; and Abdelkader and Sharqawy MH, 2022) for a detailed summary).

In order to have a (computable) model, the system (Equation 3) has to be completed with appropriate and physical meaningful boundary conditions. Since we have 6 ODEs of first-order, we therefore need 6 conditions. Suppose our *x*-direction is chosen such that the freshwater flow is positive, that is, going from the left ($x = 0$) to the right ($x = L$) as in Figures 2 and 3.

We know, that the salt flow rate at the inlet of the fresh water part vanishes, that is, $Q_{sf}(0) = 0$. Also, the salinity

$$C_d(x) = \frac{Q_{sd}(x)}{Q_{wd}(x)} \tag{11}$$

at the entrance of the salt water part is given, that is,

(12)

$C_d(0) = C_d^0$ in the co-current case (in the counter-current case it is $C_d(L) = C_d^0$). The remaining 4 conditions are given by the applied pressures. $P_f(0) = P_f^0$ is the pressure generated at the entrance of the fresh water part, $P_f(L)$ is the outlet pressure at the fresh water part where no additional pressure is applied and therefore the ambient pressure $P_f(L) = P_E$ is assumed. In the co-current case, $P_d(0) = P_d^0$ is the pressure generated by the pump at the inlet of the salt water part. Finally, $P_d(L) = P_d^L$ is the outlet pressure at the salt water part at the entrance of the turbine where the pressure decreases to the ambient pressure. We summarize the boundary conditions for the co-current case

$$Q_{sf}(0) = 0;\ C_d(0) = C_d^0$$
$$P_f(0) = P_f^0;\ P_f(L) = P_E$$
$$P_d(0) = P_d^0;\ P_d(L) = P_d^L \tag{13}$$

Since we have boundary data for C_d but not for Q_{sd}, it is convenient to introduce the new variable C_d, instead of $Q_{sd} = C_d\, Q_{wd}$. Then, system (Equation 3) reads (Di Michele et al., 2019):

$$\begin{aligned} Q_d(x) &= C_d(x)Q_{wd}(x) + Q_{wd}(x), \\ \rho_d(x) &= \frac{C_d(x)+1}{\frac{1}{\rho_s}C_d(x) + \frac{1}{\rho_w}}, \\ \Delta c_{salt}(x) &= \frac{C_d(x)}{C_d(x)+1} - \frac{Q_{sf}(x)}{Q_{sf}(x)+Q_{wf}(x)} \end{aligned} \tag{14}$$

and consequently rewriting,

$$\begin{aligned} \frac{dC_d(x)}{dx} &= -\frac{J_{s,in}(x) + J_{w,in}(x)C_d(x)}{Q_{wd}(x)}, \\ \frac{dQ_{wd}(x)}{dx} &= J_{w,in}(x), \\ \frac{dQ_{sf}(x)}{dx} &= J_{s,in}(x), \\ \frac{dQ_{wf}(x)}{dx} &= -J_{w,in}(x), \\ \frac{dP_d(x)}{dx} &= -\frac{f_{mix}(x)}{2H^2}\frac{1}{D_{HY,rect}}\frac{Q_d(x)|Q_d(x)|}{\rho_d(x)} - \frac{1}{H^2}\frac{d}{dx}\left[\frac{Q_d(x)^2}{\rho_d(x)}\right], \\ \frac{dP_f(x)}{dx} &= -\frac{f_{mix}(x)}{2H^2}\frac{1}{D_{HY,rect}}\frac{Q_f(x)|Q_f(x)|^2}{\rho_f(x)} - \frac{1}{H^2}\frac{d}{dx}\left[\frac{Q_f(x)^2}{\rho_f(x)}\right] \end{aligned} \tag{15}$$

with their dependencies on C_d.

Power and specific energy

Regarding the optimisation, we have to discuss the quantity to be optimized. We start with the net power output.

$$W_{net} = W_T - W_P^d - W_P^f \tag{16}$$

where W_T is the power produced at the turbine and W_P^d, W_P^f are the powers consumed at the pumps on the salt and fresh water side, respectively. We denote (again) with superscripts 0 and L values at the left and the right boundary, respectively. The gain at the turbine (in the following also called gross power output) is given by

$$W_T = \epsilon_T \frac{Q_d^L Y}{\rho_d^L}\left(P_d^L - P_E\right) \tag{17}$$

where ϵ_T denotes the turbine efficiency. The losses at the pumps are modelled as:

$$W_P^d = \frac{1}{\epsilon_P}\frac{Q_d^0 Y}{\rho_d^0}\left(P_d^0 - P_E\right), \quad W_P^f = \frac{1}{\epsilon_P}\frac{Q_f^0 Y}{\rho_f^0}\left(P_f^0 - P_E\right), \tag{18}$$

where ϵ_P denotes the pump efficiency.

The quantity to be optimized is the net power density per membrane area:

$$PD_{net} = \frac{W_{net}}{YL} \tag{19}$$

An alternative quantity to be optimized is the energy per total volume of the salt and fresh water flow, called the specific energy.

$$SE_{net} = \frac{W_{net}}{\frac{Q_d^0 Y}{\rho_d^0} + \frac{Q_f^0 Y}{\rho_f^0}}. \tag{20}$$

The model (Equation 14) with (Equation 13) was used in (Di Michele et al., 2019) to simulate and to optimize the co-current setting (Figure 2). Optimisation was done for both the net power and the specific energy.

The counter-current case

However, there is still the open question to evaluate the counter-current setting. It was already mentioned in (Straub et al., 2014), but a detailed comparison between the two settings is still missing. The described model allows us to do this comparison. In (Bolorunduro, 2021), a systematic comparison was started.

The difference between the two settings can be seen in Figure 2 and 3, that is, the flow in the salt part goes in the opposite direction, the pump on the saltwater part is on the right and the turbine is shifted to the left.

Therefore, we need to adjust the boundary conditions (Equation 13) to the counter-current case. We keep the *x*-

direction in the salt water part as in the co-current case (from the left to the right). The fluxes in the salt water part in the counter-current case are directed from the right to the left. The adjusted boundary conditions read:

$$Q_{sf}(0) = 0;\ C_d(L) = C_d^0$$
$$P_f(0) = P_f^0;\ P_f(L) = P_E$$
$$P_d(0) = P_d^0;\ P_d(L) = P_d^L \quad (21)$$

Power and specific energy

Finally, we need to adjust the definition of the net power components. We need to modify the turbine part (gross power (Equation 17)) to

$$W_T = \epsilon_T \frac{Q_d^0 Y}{\rho_d^0}\left(P_d^0 - P_E\right) \quad (22)$$

since the turbine has moved from the right to the left. The power part of the pumps (Equation 18) has to be modified to (the fresh water pump power remains unchanged)

$$W_P^d = \frac{1}{\epsilon_P}\frac{Q_d^L Y}{\rho_d^L}\left(P_d^L - P_E\right), \quad W_P^f = \frac{1}{\epsilon_P}\frac{Q_f^0 Y}{\rho_f^0}\left(P_f^0 - P_E\right). \quad (23)$$

The specific energy (Equation 20) remains unchanged.

The model (Equation 14) with (Equation 21) will be used to simulate and to optimize the countercurrent setting.

NUMERICAL SIMULATIONS IN THE CO- AND COUNTER-CURRENT CASE

In the co-current case, we have to solve the nonlinear boundary value problem given by Equation 14 and the boundary conditions (Equation 13). In the countercurrent case, we solve the Equation 14 with boundary conditions (Equation 21). This is done in MATLAB by using the standard solver *bvp*5*c* which is based on a finite difference method. It uses a collocation formula (Lobatto IIIa) which is implemented as a Runge Kutta formula (THE MATHWORKSINC. Solving Boundary Value Problems, 2022).

We start with a set of data which originate from (Lee et al., 1981), also used by (Di Michele et al., 2019) and (Bolorunduro, 2021) and collected in Table 1. These data are used in combination with the physical constants and input data from Table 2. The applied pressure can be found in the first row of Tables 4 and 5 for the co- and the counter-current case, respectively.

First, let us discuss the results of the simulations from a qualitative point of view. Figures 4 to 6 contain both the results for a simulation in the co-current case on the left and for the counter-current case on the right. The colors blue and green refer to quantities on the draw (salt water) and feed (sweet water) side, respectively. From a mathematical point of view, they only differ in a different allocation of the boundary conditions. Remember that in the co-current case, both fluxes are directed from the left to the right and in the counter-current case, the salt water flux is directed from the right to the left.

The total mass flow rate per width Q_f in Figure 4 is increasing in flow direction and consequently the total mass flow rate per width Q_d is decreasing in flow direction (it is positive in the co-current setting and negative in the counter-current setting). The pressures P_d, P_f in Figure 5 show a monotone behavior between the prescribed boundary conditions, the pressures decrease in flow direction.

In Figure 6, the corresponding salt and the water mass flow rates per width are shown, Q_{sd}, Q_{sf} and Q_{wd}, Q_{wf}, respectively.

Finally, in Figure 7, the related permeate water and salt fluxes can be seen, $J_{w,in}$ and $J_{s,in}$, respectively (without the mentioned color rules). Interesting to note that in the counter-current case, both permeate fluxes are not monotone, the maxima are reached in the interior.

Note that all quantities vary significantly along the membrane. The permeate flux $J_{w,in}$ reduces at $x = L$ to 1/6 of the value at $x = 0$. The pressures vary up to 50%, similar for the flow rates. This underlines the importance of resolving the quantities along the membrane instead of using a constant or some kind of mean values approach.

OPTIMISATION

So far, we have shown a typical qualitative behavior of the various quantities. For a given power station, it is desirable and important to select the operational parameters in such a way that the (net) power density and/or the specific energy are maximized. The operational parameters are the three applied boundary pressure values $P_f(0)$, $P_d(0)$, $P_d(L)$ (the value $P_f(L) = P_E$ is given as the outside pressure).

Therefore, we optimize the net power density PD_{net} in Equation 19 with respect to the 3 boundary pressures Pf(0), Pd(0), Pd(L) under the constraint of system (Equation 14). To do so, we use the MATLAB optimization algorithm named fmincon. This is a nonlinear optimization solver based on an interior-point Newton method (Di Michele et al., 2019).

Besides the possibilities in an operational phase (for a given power station), we consider also questions related to the planning phase. In that case, more parameters can be optimized to maximize net power output and/or specific energy. As an example, in addition to the applied pressures, we take the length L of the membrane module. Intuitively, we expect non-optimal values for too

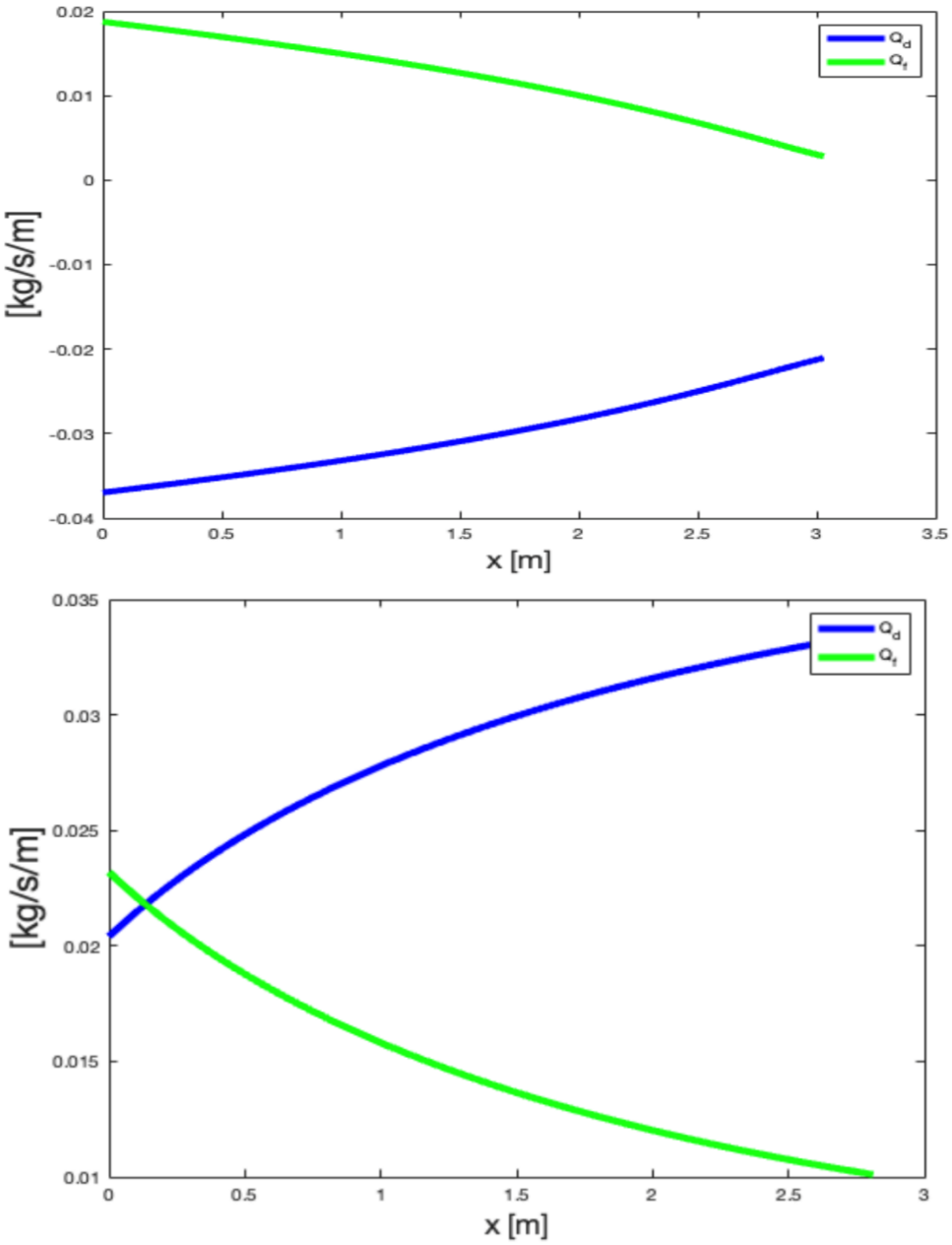

Figure 4. Total mass flow rates per width Q_d and Q_f, co-current (top) and counter-current (bottom) case.

short membranes since not enough water may permeate. Non-optimal values are also expected for too long membranes: the water on the draw side becomes too dilute versus the end (in flow direction) and thus the osmotic pressure difference to small and ineffective. And in addition, we have more friction losses. Therefore, optimal lengths are expected somewhere in between.

In this more general case, we optimize the net power output PD_{net} in Equation 19 with respect to 4 parameters, the 3 applied pressures $P_f(0), P_d(0), P_d(L)$ and the length L of the membrane using again *fmincon* in MATLAB. In a second step, we take for a given length L, the optimal pressure values and optimize the specific energy per length L with respect to L. This allows us to compare the optimal lengths for power density and specific energy for the same pressure values.

The results for the data from (Lee et al., 1981; Di Michele et al., 2019; Bolorunduro, 2021) are given in Figure 8 and in the first rows of Tables 4 and 5 for the co- and counter-current cases, respectively. In Figure 8, we see again the two cases: co-current on the left and counter-current on the right. The left picture gives the net

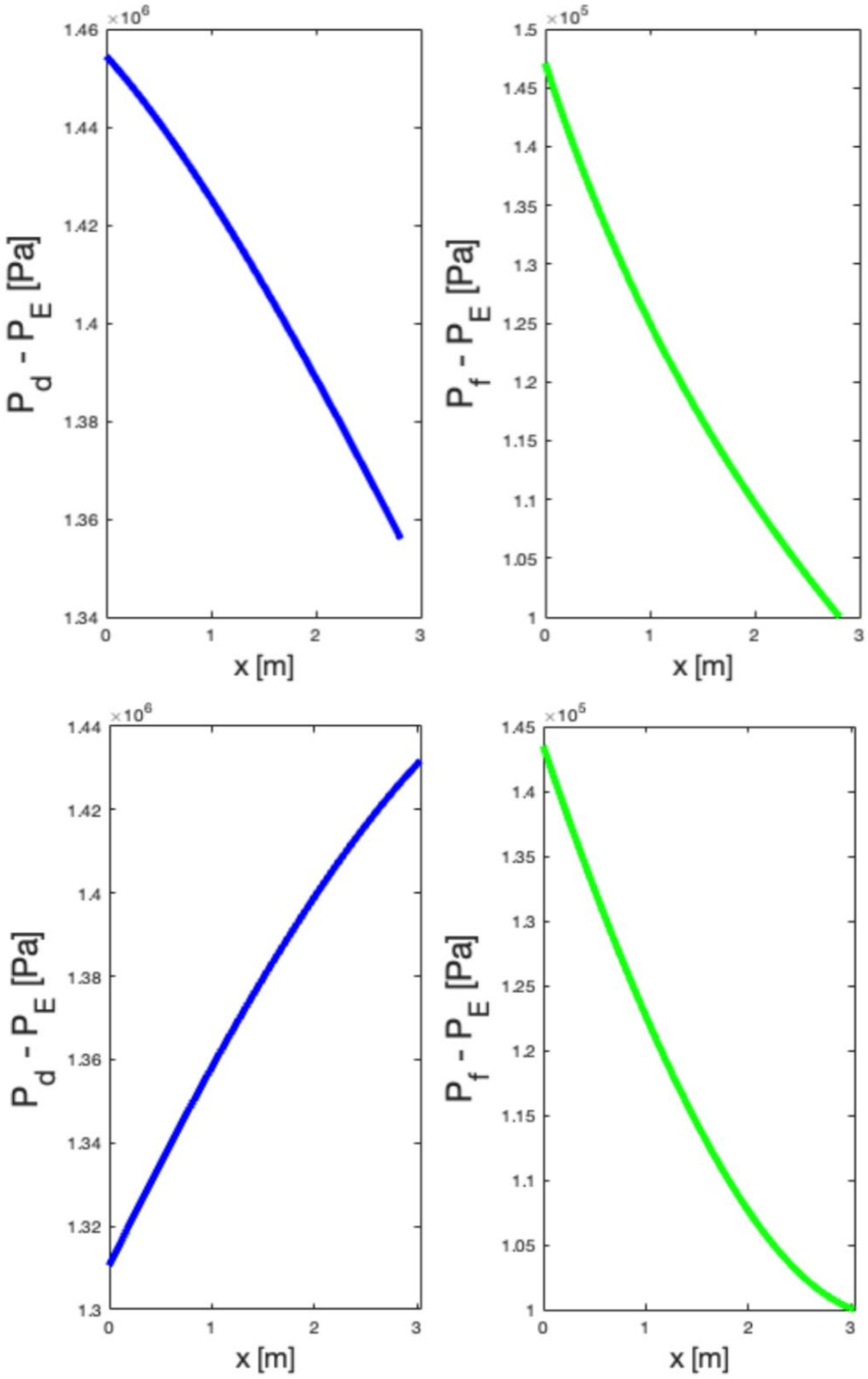

Figure 5. Total pressures $P_d - P_E$ and $P_f - P_E$, co-current (top) and counter-current (bottom) case.

and gross power density over length, the right picture gives the net and the gross specific energy over length, both according to Equation 16 without or with pump losses. We see that the net power density and the net specific energy reach optimal values at different lengths. Therefore, a decision in favor of one of the two quantities or in favor of a compromise has to be taken. To our knowledge, there is no such studies in the literature.

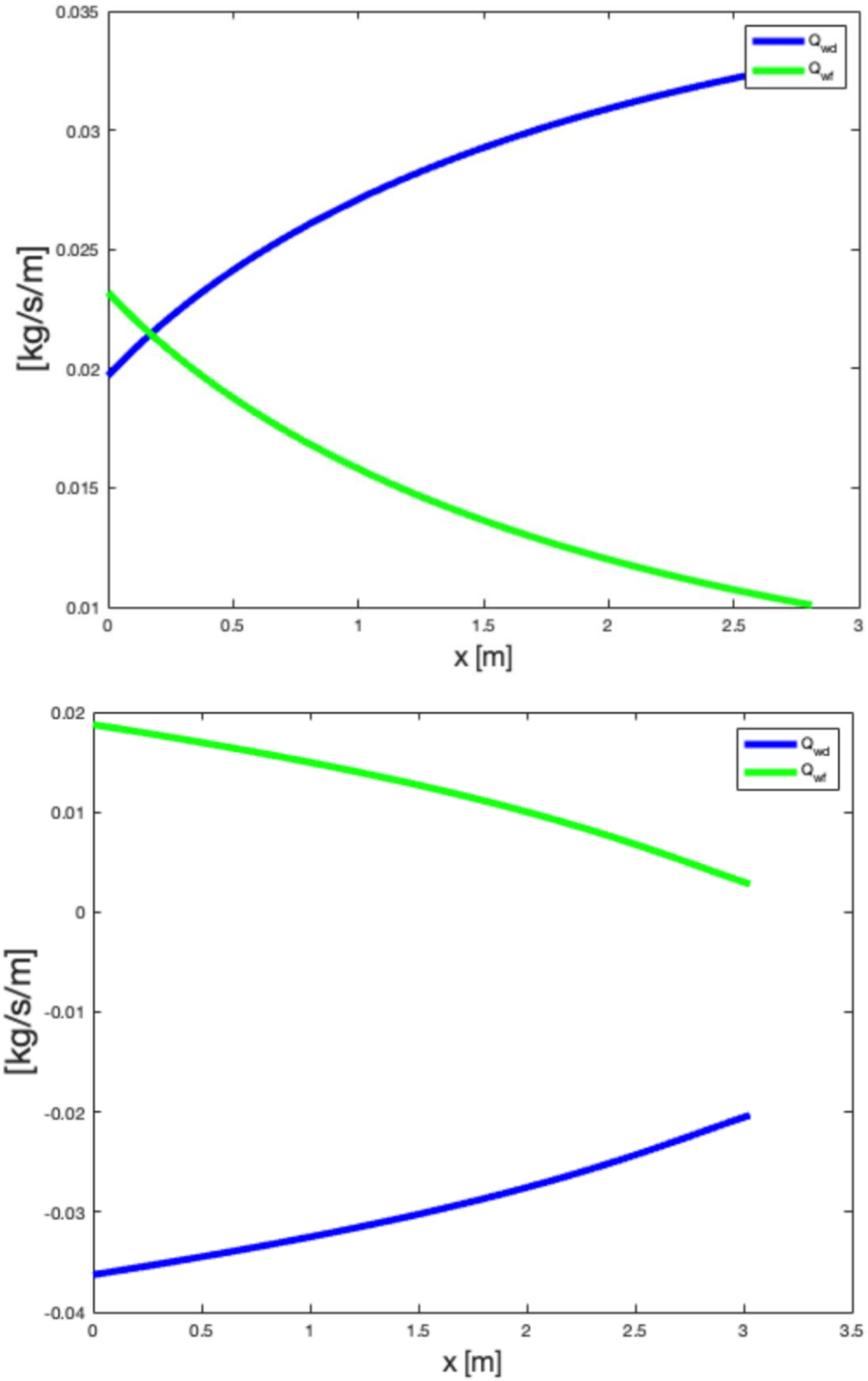

Figure 6. Water mass flow rates per width Q_{wd} and Q_{wf}, co-current (top) and counter-current (bottom) case. (Bolorunduro, 2021).

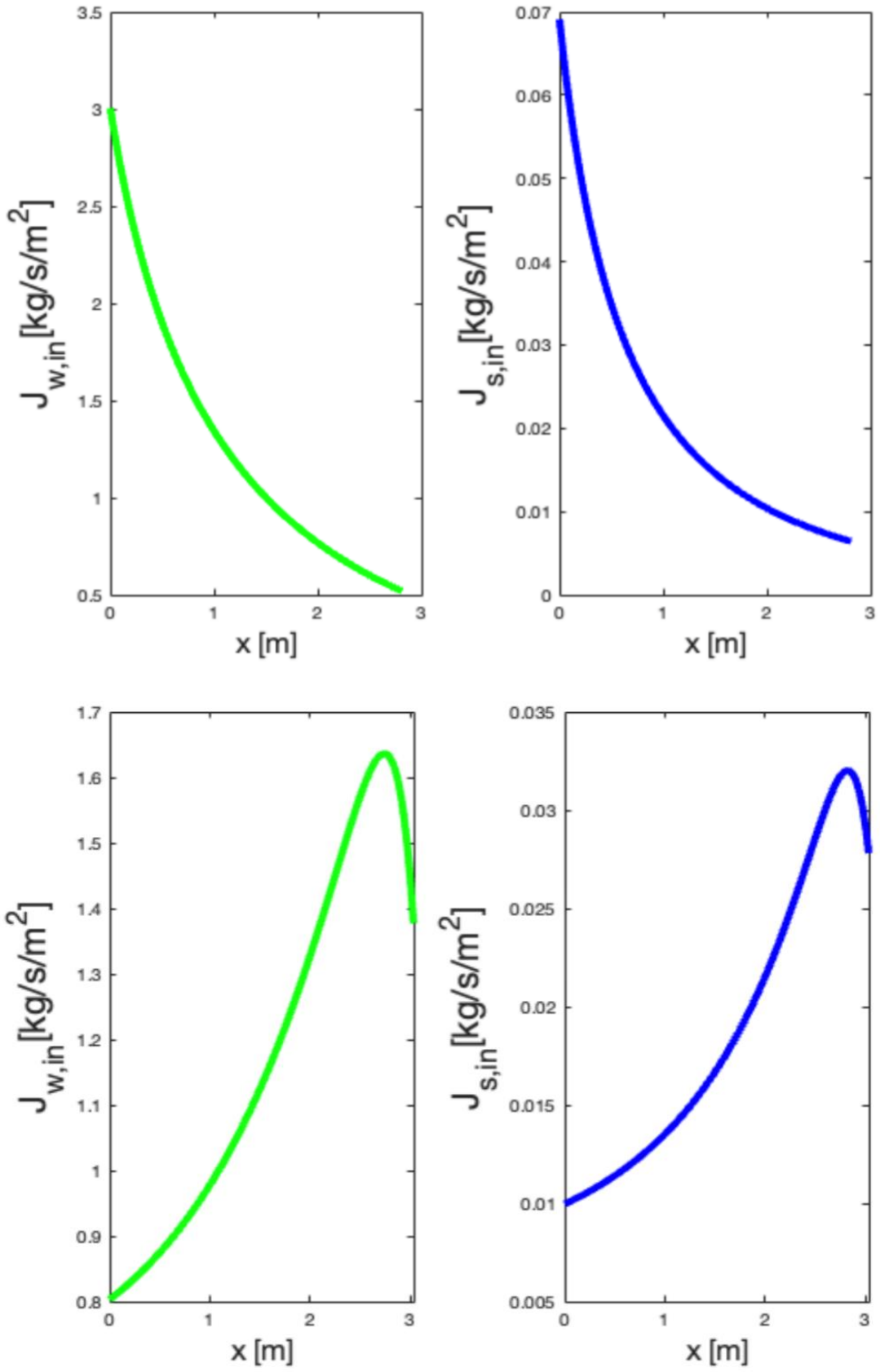

Figure 7. Permeate water J_{win} and permeate salt J_{sin} mass fluxes, co-current (top) and counter-current (bottom) case. (Bolorunduro, 2021).

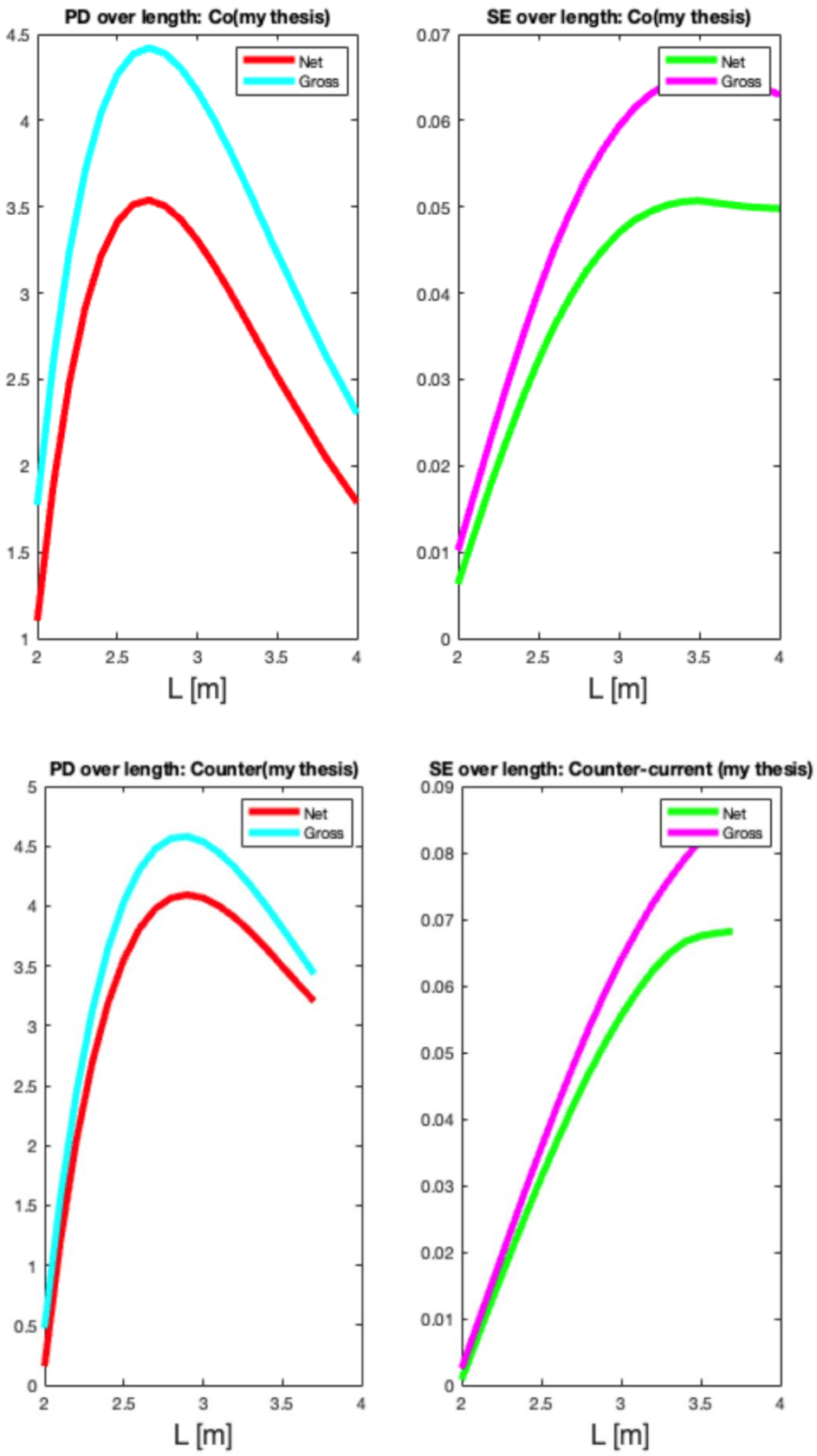

Figure 8. Power density *PD* and specific energy *SE* over length for the data from (Lee KL et al., 1981; Di Michele et al., 2019; Bolorunduro, 2021)

Table 3. Membrane parameters from the literature.

Quantity	[15, 9, 7]	[32]	[32] II	[25]
Structure parameter S (*m*)	1×10^{-4}	5.64×10^{-4}	1×10^{-4}	6.78×10^{-4}
Water permeability A (s/*m*)	2.5×10^{-9}	2.49×10^{-9}	3×10^{-9}	1.87×10^{-9}
Salt permeability B (*kg/m/s*)	given in (2.9)	3.9	3.6	1.11×10^{-7}
ICP mass transf. coef. K (m^2s/kg)	1×10^{2}	7.215×10^{-6}	7.215×10^{-6}	2.79×10^{-16}
Salt rejection coef. R (1)	0.94	not needed	non needed	not needed

However, the fact that in general power density and specific energy will give different optimal results was shown in (Straub et al., 2014) (Figure 5).

Note again, that the values vary strongly and that the optimal value is significantly better than a value for a different (but not so different) non optimal parameter choice. This means that there is lot of potential by just identifying the optimal values for a given setting. To our knowledge, there is no comparable studies in the literature.

We have done similar simulations for other parameter sets from the literature shown in Table 3. The first row in Table 3 is the set we have used up till now shown in Table 1. The two parameter sets in row 2 and 3 in Table 3 are taken from (Straub et al., 2014), the parameter set in row 4 was taken from (Maisonneuve et al., 2015). The membrane data from (Straub et al., (2014) were also used in Wang et al., 2016).

However, a direct comparison of our results to the results obtained in related papers (Straub et al. (2014; Maisonneuve et al., 2015; Wang et al., 2016) is difficult and only partly possible. As already mentioned, the models used in (Straub et al., 2014; Maisonneuve et al., 2015) are different and therefore not exactly the same selection of parameters were used. We use the salt permeability *B* in Equation 9 depending on water permeability *A*, the salt rejection *R* and the pressure differences. In (Straub et al., 2014; Maisonneuve et al., 2015), they use fixed values for *B*. Also, the mass transfer coefficients vary significantly over the various parameter sets, the one from (Lee et al., 1981) is almost historically and a few decades old. Another significant difference is the fact that most of the cited models do not include the pumps, the turbine or friction losses (Straub et al., 2014). These mentioned facts have to be considered when directly comparing the results. However, we simulated and optimized using our model including an explicit description of the pressures, friction losses, pumps and turbine and using the mentioned parameter sets, taking the mentioned constant *B* values. A significant advantage is that we can compare all these different parameter sets using the same model.

The membrane parameters used in (Straub et al., 2014) lead to the Figure 9 and to the second rows of Tables 4 and 5. In (Straub et al., 2014) also, a parameter set for a possible future membrane realization is used. That leads to the Figure 10 and to the third rows of Tables 4 and 5. Not surprisingly, the case of a future membrane from (Straub et al., 2014) performs better than the nowadays membrane. The performance is much better (16%) in power output than in specific energy (about 4%). Finally, the parameter set from (Maisonneuve et al., 2015) leads to the Figure 11 and to the last rows of Tables 4 and 5.

We see that in all cases, the maximal net power output per length is 10 to 20% better for the counter-current case. And also, the specific energy values per length for the optimal pressures and lengths (w.r.t. the power output) are better for the counter-current case. However, the optimal length is (slightly) shorter for the co-current case.

The comparison of the maximal specific energy per length values is also in favor of the counter-current case. Here, the advantage is even bigger, more than 25%. Also, the related power density values per length are better in the countercurrent case. And, again the related optimal lengths are shorter in the co-current case.

Comparing in general the power densities, we see that there is an up to 60% difference between gross and net powers (here meaning with or without pumps). In the literature, there are only very rough estimates about how much the pump power losses could be (Straub et al., 2014). Comparing the specific energies we see that the gross values are up to 2.5 times higher than the net values. The facts that the pump losses do reduce significantly the output and that the reduction is quantifiable is new relevant insight due to our modeling approach.

Trying a comparison of the values obtained in (Straub et al., 2014; Maisonneuve et al., 2015) it makes only sense to compare them to our gross values (without pump losses). However, since we have a detailed description of the $x-$ dependencies and since we include other losses such as friction losses the obtained values are expected to be lower but more realistic. In fact the obtained values are significantly lower. Thus, our approach gives quantifiable and more realistic results regarding the optimal outputs. Unfortunately, there are no comparable results in the literature, nor regarding the co- and counter-current setting, nor at the level of such a detailed model.

Table 4. PD and SE for different sets of membrane parameters: co-current setting.

Parameter	[15, 9, 7]	[32]	[32] II	[25]
P_d^0 [*bar*]	14.544	12.644	13.148	13.021
P_d^L [*bar*]	13.559	12.272	12.748	12.027
P_f^0 [*bar*]	1.471	1.293	1.308	1.211
PDtheoretical [*Wm*−2]	5.46	5.44	6.56	4.09
Maximal *PD* [Wm^{-2}]	3.49	2.46	2.87	3.74
Lenght at maximal *PD* [*m*]	2.81	1.90	1.85	2.88
SE at maximal *PD* [$kWhm^{-3}$]	0.063	0.030	0.031	0.118
SEtheoretical [*kWhm*−3]	0.099	0.066	0.070	0.128
Maximal *SE* [$kWhm^{-3}$]	0.083	0.034	0.034	0.136
SEtheoretical [*kWhm*−3]	0.181	0.086	0.086	0.207
Lenght at maximal *SE* [*m*]	3.5	2.1	2.0	3.8
PD at maximal *SE* [Wm^{-2}]	2.52	2.14	2.62	2.69

Table 5. PD and SE for different sets of membrane parameters: counter-current setting.

Parameter	[15, 9, 7]	[32]	[32] II	[25]
P_d^0 [*bar*]	13.10	11.23	11.40	12.98
P_d^L [*bar*]	14.31	11.79	12.00	14.69
P_f^0 [*bar*]	1.43	1.38	1.39	1.11
PDtheoretical [*Wm*−2]	5.46	5.44	6.56	4.09
Maximal PD [Wm^{-2}]	3.92	2.72	3.21	3.68
Lenght at maximal PD [*m*]	3.02	2.26	2.19	3.58
SE at maximal PD [$kWhm^{-3}$]	0.088	0.040	0.041	0.128
SEtheoretical [*kWhm*−3]	0.123	0.080	0.085	0.143
Maximal SE [$kWhm^{-3}$]	0.125	0.048	0.050	0.246
SEtheoretical [*kWhm*−3]	0.202	0.117	0.123	0.672
Lenght at maximal SE [*m*]	3.7	2.6	2.5	5.6
PD at maximal SE [Wm^{-2}]	3.37	2.26	2.70	1.50

Finally, we can compare the optimal results to idealized theoretical values for the power output and the specific energy. We know that in the best case, no x−dependencies, assuming homogeneous values along the flow direction, we can obtain a maximal power output of

$$PD_{theoretical} = \frac{A}{\rho_w}\frac{(\Delta\pi)^2}{4} \tag{24}$$

which only depends on the water permeability, on the mass density of water and (via $\Delta\pi$) on the salinity. The theoretical maximal specific energy is given by

$$SE_{theoretical,co} = \frac{PD_{theoretical}L}{\frac{Q_d(0)}{\rho_d(0)} + \frac{Q_f(0)}{\rho_f(0)}}, \qquad SE_{theoretical,counter} = \frac{PD_{theoretical}L}{\frac{Q_d(L)}{\rho_d(L)} + \frac{Q_f(0)}{\rho_f(0)}} \tag{25}$$

in the co- and counter-current case. Here, the effective flow rates play a role. We see that the values obtained with our more detailed model are significantly lower, from 10 to 55% in the different parameter sets for the power

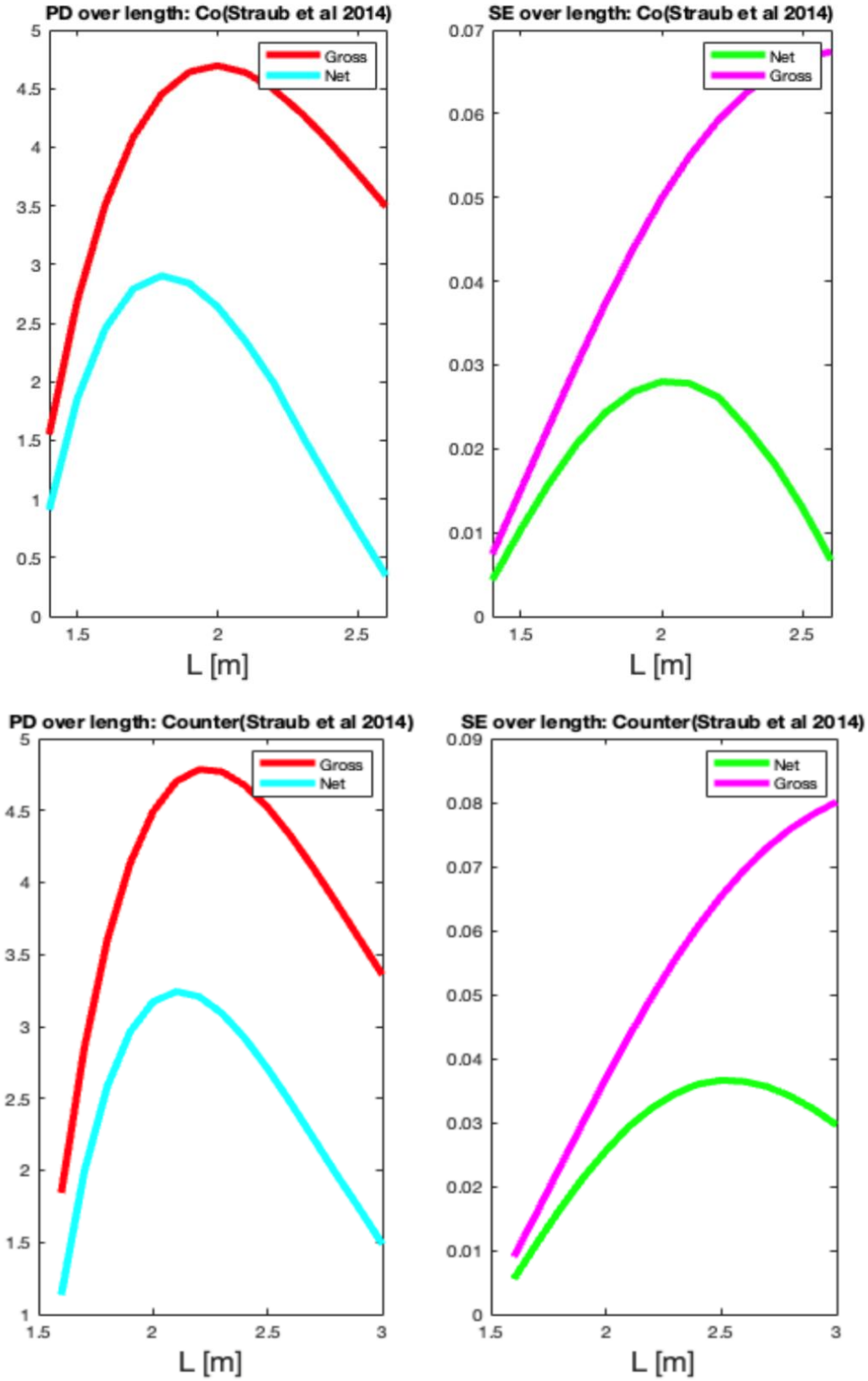

Figure 9. Power density *PD* and specific energy *SE* over length for Straub et al (2014). (Bolorunduro, 2021).

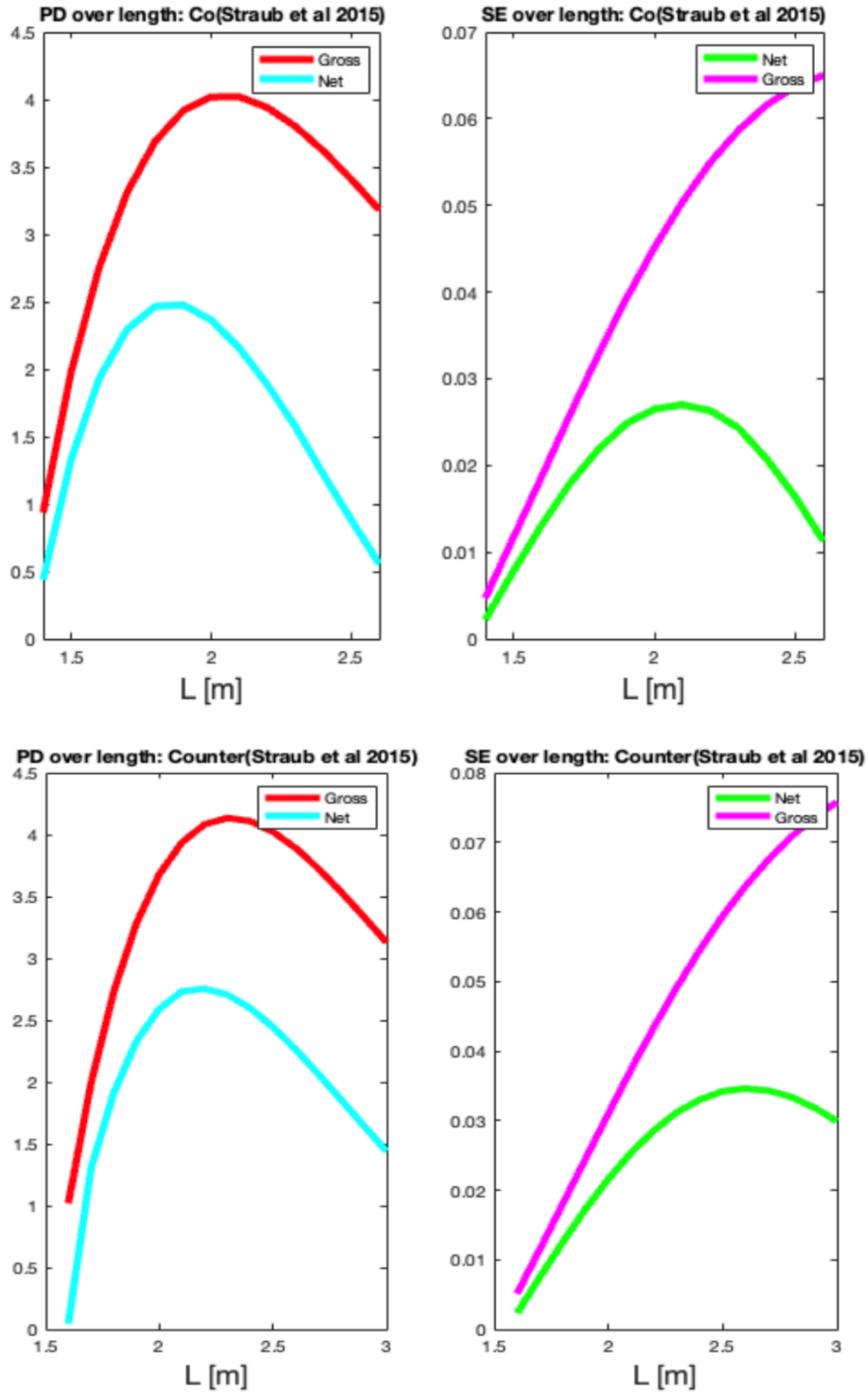

Figure 10. Power density *PD* and specific energy *SE* over length for an example of a future possible membrane in Straub et al. (2014), (Bolorunduro, 2021).

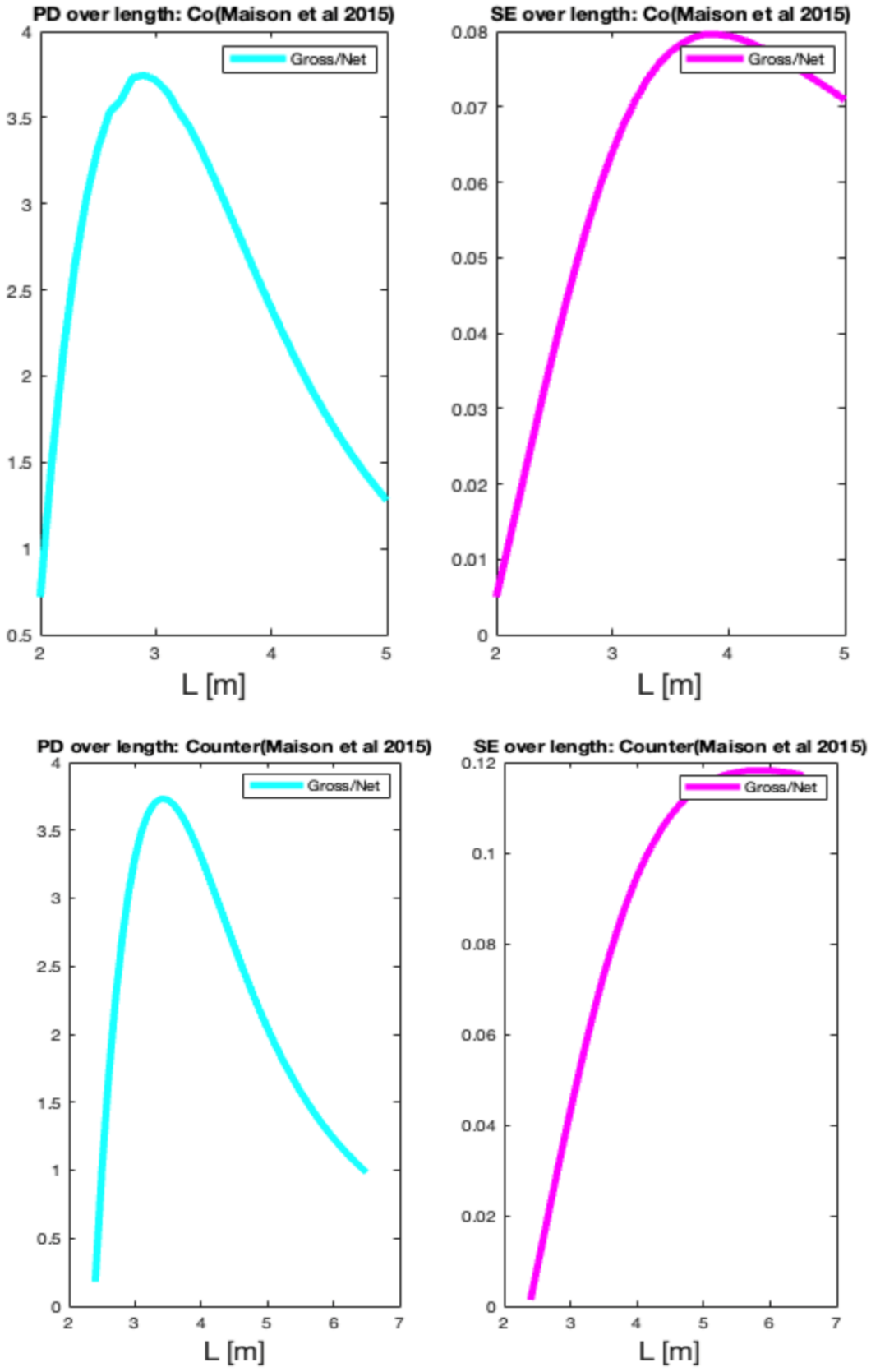

Figure 11. Power density *PD* and specific energy *SE* over length for Maison et al. (2015), (Bolorunduro, 2021).

density and even more for the specific energy.

Conclusions

We present a model which describes a PRO power station in detail, in particular, in view of real-scale PRO systems, the variation of the unknown quantities along the membrane. The model is easy to implement numerically, fast and robust to simulate and thus appropriate for optimization. This is done in this paper using state-of-the-art numerical tools.

We compare the co- and counter current settings with respect to the output power density and the specific energy. In both cases, the counter-current setting gives better values. In addition due to the more refined modeling, in particular due to the resolution of the variations along the flow direction, the simulations gives more realistic predictions, a well known drawback of former simulation results. In this sense, this model opens a variety of possibilities to improve PRO power stations.

CONFLICT OF INTERESTS

The authors have not declared any conflict of interests.

REFERENCES

Abdelkader BA, Sharqawy MH (2022). Challanges facing pressure retarded osmosis commercialisation: A short review. Energies 15(19):7325.

Achilli A, Cath TY, Childress AE (2009). Power generation with pressure retarded osmosis: an experimental and theoretical investigation. Desalination 343(1-2):42-52.

Achilli A, Childress AE (2010). Pressure retarded osmosis: From the vision of Sidney Loeb to the first prototype installation - Review. Desalination 261(3):205-211.

Alzainati N, Saleem H, Altaee A, Zaidi SJ, Mohsen M, Hawari A, Millar GJ (2021). Pressure retarded osmosis: Advancement, challenges and potential. Journal of Water Process Engineering 40:101950.

Ahmed P, Rohini (2012) Osmotic Power. http://www.yuvaengineers.com/osmotic-power-rohini-md-ahmad-peer/

Bharadwaj D, Fyles TM, Struchtrup H (2016). Multistage Pressure Retarded Osmosis. Journal of Non-Equilibrium Thermodynamics 41(4):327-347.

Bharadwaj D, Struchtrup H (2017). Large scale energy storage using multistage osmotic processes: Approaching high efficiency and energy density. Sustainable Energy and Fuels 1(3):599-614.

Bolorunduro OO (2021). Modelling, Simulation and Optimization of Pressure Retarded Osmosis (PRO) power station: co vs. counter-current setting. MSc Thesis, Department of Mathematics, Universität Hamburg, Germany.

Chen Y, Alanezi AA, Zhou J, Altaee A, Shaheed MA (2019). Optimisation of module pressure retarded osmosis membrane for maximum energy extraction. Journal of Water Process Engineering 32:100935.

Di Michele F, Felaco E, Gasser I, Serbinovskiy A, Struchtrup H (2019). Modeling, simulation and optimization of a pressure retarded osmosis power station. Applied Mathematics and Computation 353:189-207.

Gerstandt K, Peinemann KV, Skilhagen SE, Thorsen T, Holt T (2008). Membrane processes in energy supply for an osmotic power plant. Desalination 224(1):64-70

International Energy Agency (2018). 2012 Key World Energy. Statistics, http://www.iea.org/publications/freepublications/, IEA.

Kim J, Jeong K, Park MJ, Shon HK (2015). Recent Advances in Osmotic Energy Generation via Pressure-Retarded Osmosis (PRO): A Review. Energies 8(10):11821-11845

Lee KL, Baker RW, Lonsdale HK (1981). Membranes for power generation by pressure-retarded osmosis. Journal of Membrane Science 8(2):141-171

Lin S, Straub AP, Elimelech M (2014). Thermodynamic limits of extractable energy by pressure retarded osmosis. Energy and Environmental Science 7(8):2706-2714.

Loeb S (1976). Production of electric power by mixing fresh and salt water in hydroelectric pile. Journal of Membrane Science 1:49-63

Loeb S, Norman R (1975). Osmotic power plants. Science 189(4203):654-655

Logan BE, Elimelech M (2012). Membrane-based processes for sustainable power generation using water. Nature 488(7411):313-319.

Maisonneuve J, Pillay P, Laflamme CB (2015). Pressure osmotic power system model considering non-ideal effects. Renewable Energy 75:416-424.

Mathworks Help Centre, Fmincon, THEMATHWORKS INC.FMINCON (2022). https://www.mathworks.com/help/optim/ug/fmincon.html

Norman R (1974). Water salination: A source of energy. Science 186:350-352.

O'Toole G, Jones L, Coutinho C, Hayes C, Napoles M, Achilli A (2016). River-to-sea pressure retarded osmosis: Resource utilization in a full-scale facility. Desalination 389:39-51.

Pattle R (1954). Production of electric power by mixing fresh and salt water in hydroelectric pile. Nature 174(4431):660-660.

Pattle R (1974). Water salination: a source of energy. Science 186(4161):350-352.

Ruiz-Garcia A, Tadeo F, Nuez I (2022). Simulation tool for fullscale PRO systems using SWMMs. Desalination 541:116025.

Senthil S, Senthilmurugan S (2016). Reverse osmosis-pressure retarded osmosis hybrid systems: modelling, simulation and optimization. Desalination 389:78-97

Straub AP, Lin S, Elimelech M (2014). Module-Scale Analysis of Pressure Retarded Osmosis: Performance Limitations and Implications for Full-Scale Operation. Environmental Science and Technology 48:1243512444.

Struchtrup H (2014). Thermodynamics and Energy Conversion. Springer, Heidelberg.

Sundaramoorthy S, Srinivasan G, Murthy DVR (2011). An analytical model for spiral wound reverse osmosis membranes modules: Part I-Model development and parameter estimation. Desalination 280(1-3):403-411.

Sung-Soo H, Won R, Myung-Suk C, Seung OL, Gui-Yung C (2014). Numerical studies on the pressure-retarded osmosis (PRO) system with the spiral wound module fo power generation. Desalination and Water Treatment 52(34-36):6333-6341.

Torleif H, Thorsent ET (2009). Semi-permeable membrane for use in osmosis, and method and plant for providing elevated pressure by osmosis to create power. US Patent No 7,566,402.

Wang Z, Hou D, Lin S (2016). Gross vs. net energy: Towards a rational framework for assessing the practical viability of pressure retarded osmosis. Journal of Membrane Science 503:132-147.

Yang W, Song L, Zhao J, Chen Y, HU B (2018). Numerical analysis of performance of ideal counter-current flow pressure retarded osmosis. Desalination 433:41-47.

Appendix 1. List of symbols.

Quantity	Symbol	Dimension
Height of the membrane unit	H	m
Width of the membrane unit	Y	m
Length of the membrane unit	L	m
Position along the membrane unit	x	m
Salt flow rate per width in fresh water	Q_{sf}	$kgs^{-1}m^{-1}$
Water flow rate per width in fresh water	Q_{wf}	$kgs^{-1}m^{-1}$
Flow rate per width in fresh water	Q_f	$kgs^{-1}m^{-1}$
Salt flow rate per width in salt water	Q_{sd}	$kgs^{-1}m^{-1}$
Water flow rate per width in salt water	Q_{wd}	$kgs^{-1}m^{-1}$
Flow rate per width in salt water	Q_d	$kgs^{-1}m^{-1}$
Water flux through the membrane from fresh to salt water	Jw,in	$kgs^{-1}m^{-2}$
Salt flux through the membrane from salt to fresh water	Js,in	$kgs^{-1}m^{-2}$
Salt water mass density	ρ_d	kgm^{-3}
Fresh water mass density	ρ_f	kgm^{-3}
Water mass density	ρ_w	kgm^{-3}
Salt mass density	ρ_s	kgm^{-3}
Water molecular weight	M_w	$kskmol^{-1}$
Salt molecular weight	M_s	$kgkmol^{-1}$
Salt water pressure	P_s	Pa
Fresh water pressure	P_f	Pa
Pressure difference	ΔP	Pa
Salt water part osmotic pressure	π_s	Pa
Fresh water part osmotic pressure	π_f	Pa
Osmotic pressure difference	$\Delta\pi$	Pa
Pump power salt water part	W_Pd	W
Pump power fresh water part	W_Pf	W
Turbine power	W_T	W
Net power	W_{net}	W
Power density	PD	Wm^{-2}
Specific energy	SE	Wsm^{-3}
Salinity in the salt water part	C_d	1
Salt concentration difference	Δc	1
Reynolds number	$ReH,f/d$	1
Friction coefficient	$fmix,f/d$	1
Temperature	T_0	K
Water gas constant	R_w	$Jkmol^{-1}K^{-1}$
Saltwater viscosity	σ	$kgs^{-1}m^{-1}$
Pump/turbine efficiencies	ϵP, ϵT	1
Salt Rejection	R	1
Water permeability	A	sm^{-1}
Salt permeability coefficient	B	$kgs^{-1}m^{-2}$
ICP mass transfer coefficient	K	m^2skg^{-1}

Source: Di Michele et al., 2019, Bolorunduro,, 2021.